Nocturnal cold air drainage and pooling in a tropical forest

Michael L. Goulden,[1] Scott D. Miller,[1] and Humberto R. da Rocha[2]

Received 1 April 2005; revised 21 October 2005; accepted 13 January 2006; published 26 April 2006.

[1] The usefulness of eddy covariance for understanding terrestrial carbon exchange has been hampered by uncertainty over the magnitude and causes of a systematic underestimation of CO_2 efflux on calm nights. We combined in situ measurements of the temperature, wind and CO_2 profile with nocturnal Land Surface Temperature (LST) imagery from the Advanced Spaceborne Thermal Emission and Reflection Radiometer (ASTER) to infer the patterns of cold air drainage in an Amazonian tropical forest. The meteorological tower was located on a flat plateau that sloped gently to the southwest. The vertical profile from 0 to 64 m above ground level was divisible into two air parcels at night: a warm, low CO_2, upper parcel and a cool, high CO_2, lower parcel that was stable with respect to the upper parcel. The nocturnal wind direction of the upper parcel was from the east, a pattern that is consistent with the general circulation, whereas the wind direction of the lower parcel was from the northeast, a pattern that implies drainage down the local topographic gradient. The nocturnal patterns of LST were closely related to local topography and land use. In general, a nearby river was warm, gullies were cold, plateau centers were cold, stream drainages were cold, pastures were particularly cold, and upper slopes and plateau edges were warm. The in situ temperature and wind observations, combined with the observed relationship between elevation and nocturnal LST and the occurrence of warm thermal belts extending inward from the edges of plateaus, imply that cold air drainage occurs on clear nights. The slope of the relationship between LST and elevation varied between nights, indicating that the degree of thermal stratification, and possibly the extent of cold air drainage, also varied. The night-to-night variation in stratification across the landscape was correlated with the vertical temperature gradient at the tower but not the above-canopy friction velocity (u*). Criteria associated with vertical temperature gradients may prove better than u* for screening nocturnal eddy covariance observations to eliminate periods that underestimate CO_2 flux.

Citation: Goulden, M. L., S. D. Miller, and H. R. da Rocha (2006), Nocturnal cold air drainage and pooling in a tropical forest, *J. Geophys. Res.*, *111*, D08S04, doi:10.1029/2005JD006037.

1. Introduction

[2] The use of long-term eddy covariance to calculate the annual net CO_2 exchange by terrestrial ecosystems has become widespread in the last decade [*Wofsy et al.*, 1993; *Valentini et al.*, 2000; *Baldocchi et al.*, 2001]. Much of this research has been motivated by the need to identify the locations and causes of terrestrial carbon sequestration [*Tans et al.*, 1990]. However, the utility of long-term eddy covariance for understanding terrestrial carbon exchange has been hampered by uncertainties over the accuracy of the calculated annual integral and, in particular, the magnitude and causes of a possible systematic underestimation of CO_2 efflux on calm nights [*Goulden et al.*, 1996; *Lee*, 1998; *Massman and Lee*, 2002; *Miller et al.*, 2004].

[3] The daily or annual net CO_2 exchange at a site is the relatively small difference of two larger fluxes: the daytime uptake of CO_2 and the nocturnal loss of CO_2 by respiration. Calculation of the annual integral is sensitive to measurement biases from day to night; a modest systematic underestimation of nighttime efflux relative to daytime uptake will cause a large overestimation of annual uptake. Eddy covariance provides a measure of the vertical turbulent flux above a site, which may or may not be equivalent to the production or consumption of CO_2 by the site's biota. Surface heating during daytime results in convection and vigorous vertical transport. The movement of CO_2 into or out of an ecosystem is dominated by vertical turbulent transport during convective periods, and eddy covariance provides a valid measure of biotic metabolism during daytime. In contrast, surface cooling at night often suppresses vertical transport, and CO_2 may move into or out of a site by mechanisms other than turbulent transport. The suppression of vertical transport, and possible increases in horizontal advective or drainage flux, may cause eddy covariance to systematically underestimate biotic metabolism on calm and clear nights. In turn, this systematic bias

[1]Department of Earth System Science, University of California, Irvine, California, USA.
[2]Department of Atmospheric Sciences, University of Sao Paulo, Sao Paulo, Brazil.

0148-0227/06/2005JD006037$09.00

creates a large uncertainty in the calculated annual net exchange.

[4] The possibility of a systematic bias in measurement from day to night was recognized by *Wofsy et al.* [1993] and explored by *Goulden et al.* [1996] and *Black et al.* [1996], among others. *Goulden et al.* [1996] concluded that eddy covariance underestimates biotic flux at night as a function of the vertical mixing above a site, and suggested that this underestimation might result from advective or drainage flows. However, *Goulden et al.* [1996] did not investigate the physical cause of nocturnal flux underestimation, and provided no direct evidence that a net advective flux occurs. Rather, they attempted to bypass the problem by computationally replacing the fluxes during calm periods with those observed during windier periods. Subsequent research focused on understanding the mechanistic causes of nocturnal flux underestimation, with an emphasis on several terms in the continuity equation that had been assumed unimportant [*Lee*, 1998; *Finnigan*, 1999; *Baldocchi et al.*, 2000]. The conventional eddy covariance approach assumes that transport is vertical and one-dimensional, whereas transport on calm nights likely involves a three-dimensional combination of horizontal and vertical flow [*Finnigan*, 1999]. Several field experiments have now provided direct evidence of a significant net advective flux at night [*Feigenwinter et al.*, 2004; *Aubinet et al.*, 2003; *Turnipseed et al.*, 2003; *Staebler and Fitzjarrald*, 2004].

[5] In practice, horizontal or vertical drainage fluxes are difficult to characterize since they require observations at many locations with high precision. A potentially complementary approach to the in situ instrumentation strategy that has been the focus of past field experiments is the use of thermal imagery to characterize the spatial relationship between topography and Land Surface Temperature (LST). Tower-based thermal imagery has been used at a small scale to determine the relationships between microtopography and temperature [*Radke and Delany*, 2002]. At a larger scale, the Advanced Spaceborne Thermal Emission and Reflection Radiometer (ASTER) has a high spatial resolution (90 m) and is routinely operated at night, making it suitable for investigating how LST varies across the landscape. In this paper we combine ASTER imagery with in situ measurements of the meteorological conditions to infer the patterns of cold air drainage in an Amazonian tropical forest. Our immediate goal is to use the combination of ASTER imagery and in situ measurements to demonstrate and better understand the nocturnal occurrence of a thermal inversion and, by inference, cold air drainage. Our long-term goal is to better understand how to use the meteorological observations made at a single site to diagnose or correct the underestimation of CO_2 efflux on calm nights.

2. Methods

2.1. Site

[6] The study was conducted in the FLONA Tapajós study area of the Large-Scale Biosphere-Atmosphere Experiment in Amazonia (LBA [*Keller et al.*, 2004]), approximately 70 km south of Santarem, Pará Brazil (Figure 1) [*Miller et al.*, 2004; *Goulden et al.*, 2004; *da Rocha et al.*, 2004]. The in situ field measurements were made at the km-83 micrometeorological tower (south $-3°1'3.0''$, west $-54°58'15.0$). The remote sensing and spatial analysis focused on areas within 10 to 15 km of the tower.

[7] The vegetation was closed tropical forest with canopy emergents on flat upland terrain [*Hernandez Filho et al.*, 1993]. The forest was semidecidous, with mostly evergreen and a few deciduous species. Forest extended 5 km to the east before reaching pasture on the far side of the nearest paved road (BR-163), 8 km to the south before reaching pasture, and 40 km to the north before reaching pasture (Figure 1). An area extending 2 to 3 km east of the tower was selectively logged in September 2001 as part of a larger experiment. The logging removed ~5% of the aboveground biomass and had only a minor effect on the forest's meteorology. In the current paper we combine the before- and after-logging observations.

2.2. In Situ Meteorological and Eddy Covariance Measurements

[8] The in situ methods were described in detail by *Goulden et al.* [2004], *Miller et al.* [2004], and *da Rocha et al.* [2004]. The measurements were made from a 67-m-tall, 46-cm cross section tower (Rohn 55G, Peoria, Illinois). Additional instruments were mounted on one of three 2-m tripods installed on the forest floor. Power was provided by one of two 20-kVA diesel generators located 800-m south of the tower.

[9] The turbulent fluxes of sensible heat, latent heat, CO_2, and momentum at 64 m above ground level (agl) were determined with the eddy covariance technique [*Baldocchi et al.*, 1988; *Wofsy et al.*, 1993]. The signals directly required for flux calculation were digitized and stored at 4 Hz. Wind and temperature were measured with a 3-axis sonic anemometer pointed due east (Campbell Scientific, Logan, Utah). The molar densities of CO_2 and H_2O at 64 m were measured with two independent InfraRed Gas Analyzers (IRGAs); an open-path instrument (LI-COR LI7500, Lincoln, Nebraska) at 64 m and a closed path instrument (LI-COR LI7000, Lincoln, Nebraska) in a hut at the base of the tower that sampled air drawn down a heated 9.5-mm inner diameter 75-m-long Teflon PFA tube. The CO_2 fluxes for both the open and closed path IRGAs were calculated as the 30-min covariance of the vertical wind velocity (w') and the CO_2 mixing ratio after subtracting the 30-min mean (c'). The time lag for the closed path IRGA was determined by maximizing the correlation between the fluctuations in air temperature (T') and c'. The fluxes were rotated to the plane with no mean vertical wind [*McMillen*, 1988]. *Miller et al.* [2004] compared the results from the open- and closed-path systems, and discussed the sensitivity of calculated flux to averaging time, detrending, rotation, and method of open-path density correction.

[10] A third IRGA (LI-COR LI7000 or, LI800 before December 2000, Lincoln, Nebraska) sequentially measured the densities of CO_2 and H_2O at 12 heights (0.1, 0.35, 0.7, 1.4, 3, 6, 10.7, 20, 35, 40, 50, 64-m agl) every 48 min. Four standard liters of air per minute were drawn through a 2 μm filter at each height, down 5.5-mm inner diameter polyethylene lined tubing (Furon Dekabon 1300), through a solenoid manifold in an enclosure at the base of the tower (Parker General Valve, Fairfield, New Jersey), into the equipment hut, and through the IRGA cell. The half-hourly

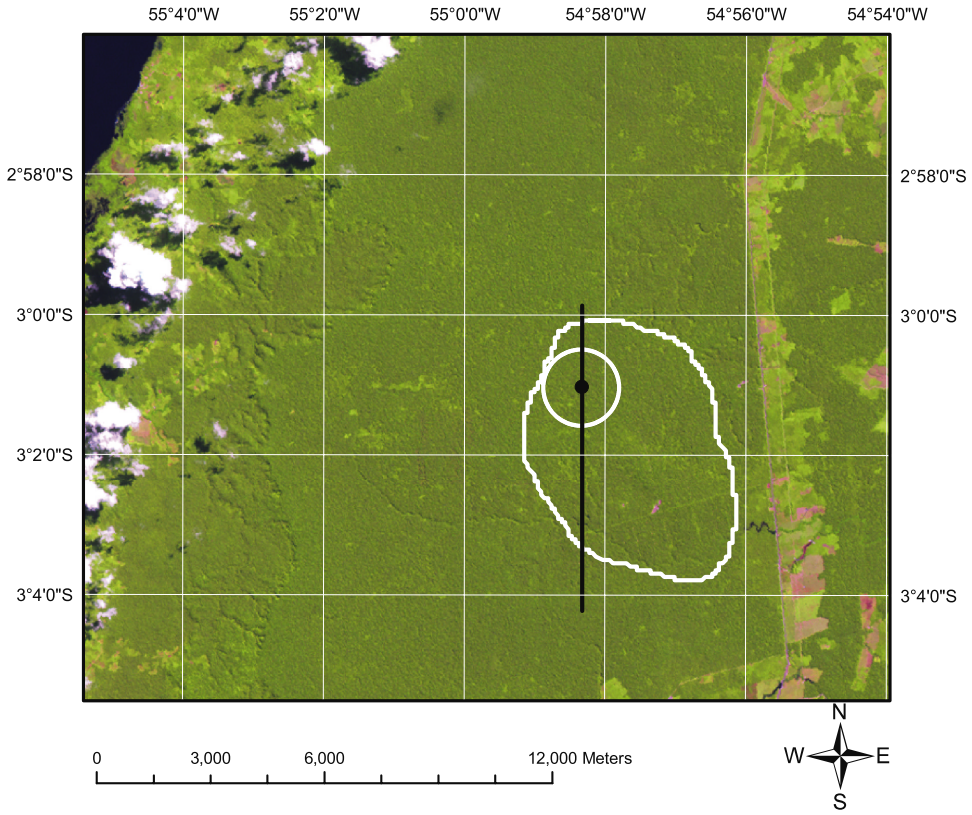

Figure 1. Landsat ETM+ for 30 July 2001. The image is false color (RGB bands 5, 4, and 3). Dense vegetation appears as green, water appears as dark blue, and bare soil or open pasture appear as red. The Tapajos River appears in the top left hand corner; the nearest road (BR-163) and associated areas of pasture and cropland traverse the image from north to south. The km 83 tower site is shown with a solid circle. A 1 km radius circle around the tower is shown in white. An 8 km transect passing the tower is shown in black. A ~30 km^2 region of interest that surrounds the tower is shown in white.

change in CO_2 beneath 64 m was calculated by vertical integration and temporal differentiation (storage [*Wofsy et al.*, 1993]).

[11] The horizontal wind speed and direction at 64 m agl was calculated from the main 3-axis sonic anemometer. The horizontal wind speeds and directions at 30, 20, and 1.3 m agl were measured with 2-axis sonic anemometers (Met One 035A, Grants Pass, Oregon). The 2-axis anemometers operated intermittently, and exhibited occasional spiking on the u or v axis as indicated by anomalously high wind velocities and biased wind directions. Our analysis of horizontal wind focused on the periods when the instruments produced unambiguously valid data. The horizontal wind speeds and directions measured by the 2-axis anemometers were recorded at 1 Hz and then converted into u and v components for averaging to 30-min intervals. The air temperatures at 64, 40, 30, 20, 10 and 2 m agl were measured with ventilated thermistors (Met One 076B, Grants Pass, Oregon; Campbell Scientific 107, Logan, Utah).

[12] The data acquisition computer was equipped with a high-precision clock that maintained the time within 1 min of UTC on the basis of periodic checks with a GPS. All in situ data were collected with a UTC time stamp, which allowed us to temporally synchronize the in situ and satellite data during subsequent analyses.

2.3. Image Analysis

[13] We combined nocturnal images of Land Surface Temperature (LST) from the Advanced Spaceborne Thermal Emission and Reflection Radiometer (ASTER) with a Digital Elevation Model (DEM) from the Shuttle Radar Topography Mission (SRTM) to infer the patterns of cold air pooling in the area around the km-83 tower. ASTER was selected because it has a high spatial resolution (90 m) and is routinely operated at night. In contrast, the Landsat Enhanced Thematic Mapper Plus (ETM+) has an even higher thermal resolution (60 m) but is usually switched off at night, and the Moderate Resolution Imaging Spectroradiometer (MODIS) is operated at night but has a much coarser thermal resolution (1 km). The SRTM DEM was selected as the only high-resolution (90 m) elevation data set available for the site.

[14] All spatial analyses were done relative to a 30 July 2001 ETM+ image that we took as our reference image (Figure 1; Path/Row: 227/62; Level 1G tiff image in UTM 21S from the Earth Resources Observation Systems (EROS) Data Center). The location of the km-83 site on the ETM+

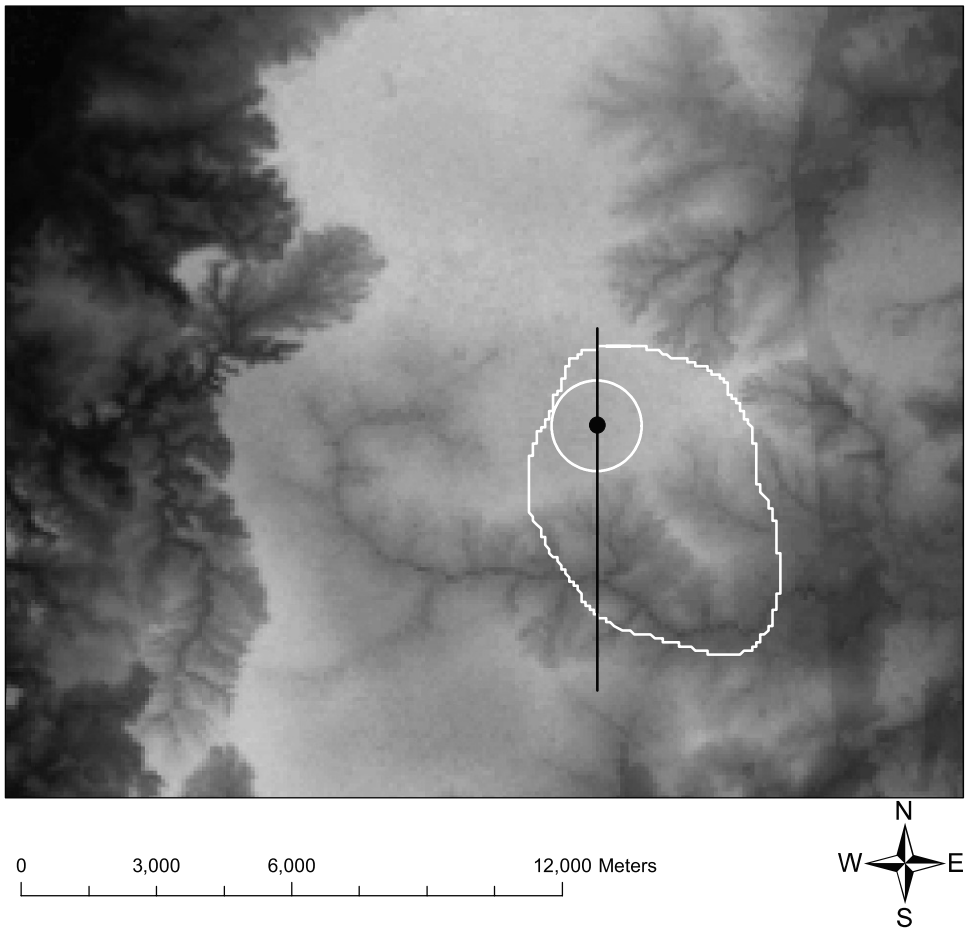

Figure 2. Local topography as determined by the Shuttle Radar Topography Mission (SRTM). The tower and regions of interest are shown as in Figure 1. Lower-elevation sites are darker; higher-elevation sites are lighter. The elevation ranges from ~5 m above sea level at the Tapajos River to ~195 m asl in the center of the plateau. The spatial resolution of the SRTM data is 90 m. The SRTM recorded the height of the canopy, resulting in a step change in elevation at the edges of the forest along BR-163.

reference image was determined from easily observable landmarks on a pan-sharpened IKONOS image for 11 November 2001 that we obtained from the EOS-Webster Earth Science Center and coregistered to the ETM+ base map. We used a common set of prominent landscape features that were apparent in all types of imagery as control points to register the SRTM and ASTER images to the ETM+ reference image. These points included the corners of pastures, branching points of small rivers, and intersections between streams and roads. The Normalized Difference Vegetation Index (NDVI; a measure of canopy density and the interception of light by green vegetation) was calculated for the 30 July 2001 ETM+ image from the Red and Near InfraRed bands (bands 3 and 4).

[15] We obtained 90-m SRTM data as $1^\circ \times 1^\circ$ tiles in hgt format from the EROS Data Center, mosaiced the tiles, and then reprojected and registered the DEM to the ETM+ reference image at 90-m resolution. We started our analysis of ASTER imagery by obtaining all of the nocturnal L1B (AST03) scenes available for the site from the EROS Data Center. We then screened these images to select unambiguously cloud free conditions, and focused our subsequent analyses on Land Surface Kinetic Temperature images (AST08) for 20 October 2003, 0207 UTC; 8 August 2003, 0212 UTC; 15 September 2002, 0208 UTC; 3 February 2002, 0209 UTC; 1 December 2001, 0211 UTC; 21 October 2001, 0218 UTC; and 27 August 2001, 0214 UTC that we obtained from the EROS Data Center. The local sunset occurs at 2200 UTC year-round. About half of the nocturnal images were cloud free, with a marked increase in nocturnal cloudiness in the wet season (approximately January through June) and a decrease in the dry season. This pattern is consistent with our observations of nocturnal net radiation, and implies that radiational cooling of the surface is frequent at night, especially during the dry season. Ground fog often occurs at the tower site shortly after rain, and is reported to occur in nearby pastures on clear nights [*Acevedo et al.*, 2004], a pattern that is consistent with the cool LST observed in these areas. We are unable to fully evaluate how fog would affect our analyses, though we expect that the effect would be minor since ground fog would presumably have a similar temperature and elevation as the nearby vegetation. High fog would probably show up as an anomalously cold patch, and we would have excluded the image from analysis.

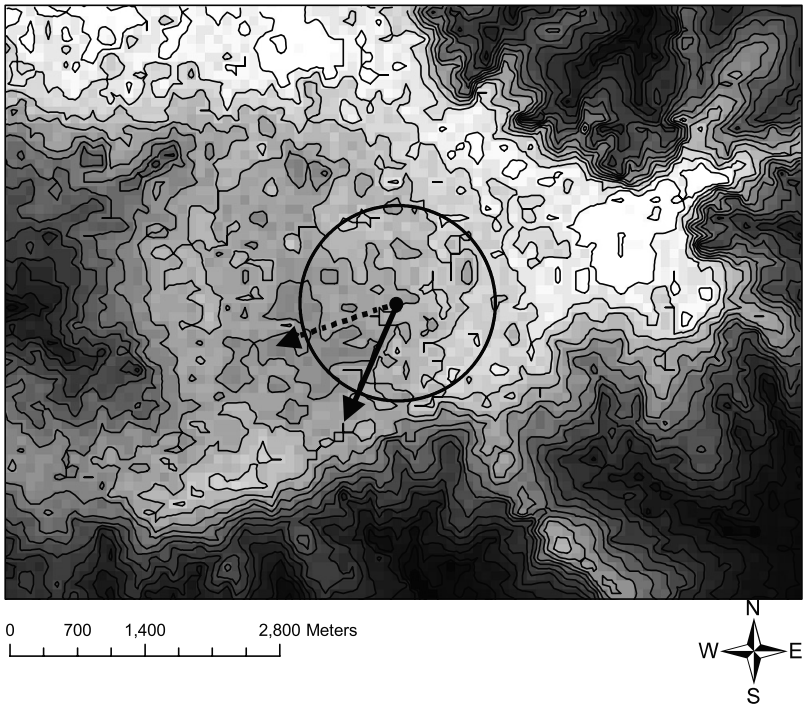

Figure 3. Topographic contours at 5-m intervals around the eddy flux tower as determined by the Shuttle Radar Topography Mission (SRTM). The km 83 tower site is shown with a solid circle. A 1 km radius circle around the tower is shown as a black circle. The absolute elevation determined by the SRTM is shown on a stretched gray scale, with black corresponding to an elevation of 135 m asl and white to an elevation of 195 m asl. The dashed arrow shows the modal wind direction at 20 m agl during daytime; the solid arrow shows the modal 20-m wind direction at night.

[16] The on-demand AST08 images were calculated using the climatology setting for the aerosol source and the NCEP setting for the Ozone and Temperature sources. We then reprojected and registered the 90-m AST08 images to the ETM+ reference image at 90-m resolution. The seven coregistered AST08 scenes were stacked with the SRTM DEM to compare LST with elevation. Our spatial analyses focused on three regions of interest (Figure 1): (1) a 1 km radius circle centered on the tower; (2) an 8-km north-to-south transect that traversed a flat region in the north and a broad, 80-m deep stream valley in the south; and (3) a $\sim$30 km^2 area around the tower with 3576 90-m pixels that was drawn to include a range of elevations within the local drainage around the tower. All of the regions of interest were forest except for a small clear patch $\sim$4 km southeast of the tower that is used as a source of latarite for road construction (Figure 1). The numerical values for each pixel in the regions of interest were output to ASCII files and further analyzed in either MATLAB (MATLAB version 6.5, The Mathworks, Inc. Natick, Massachusetts) or Excel (Excel 2000, Microsoft, Redmond, Washington). All other spatial analyses were done in either ENVI (ENVI version 4.0, Research Systems, Inc. Boulder, Colorado) or ArcGIS (ArcINFO 9.0, ESRI, Redlands, California).

[17] ASTER's narrow path and small pixel mean that it must be tasked, and, as a result, only a few ASTER images are available for most locations. Our study site was affiliated with the LBA-ECO project, and we were fortunate that ASTER was tasked repeatedly to record nocturnal thermal images of the region. Since an extensive collection of ASTER imagery is unlikely to be available for most tower sites, we explored the possibility of using the much coarser but more widely available MODIS thermal imagery. Unfortunately, MODIS LST (MOD11) is not calculated for pixels that have a greater that 1% chance of cloud contamination [*Wan*, 1999], a very stringent criteria that precluded the use of MOD 11 at km 83. As a result, we focused our analyses on MODIS Level 1B band 31 radiance (MOD02). After registering and reprojecting the MOD02 images to UTM 21S, and screening to exclude images with cloud cover and ones that were centered more than 5° latitude from the site, we found a relationship between MODIS thermal radiance and SRTM elevation that was qualitatively similar to that observed between ASTER LST and elevation. We do not show results from the MODIS analyses, since they did not add anything beyond what we learned from ASTER. Nonetheless, we want to point out that MODIS imagery may prove useful for understanding the development of nocturnal stratification at sites where ASTER imagery is unavailable.

3. Results and Discussion

3.1. Topography

[18] The tower was located on a flat plateau that extended 6 to 10 km to the west before reaching an escarpment that dropped 200 m over 5 km to the Tapajos River (Figures 1 and 2). The plateau extended for many km to the south, east,

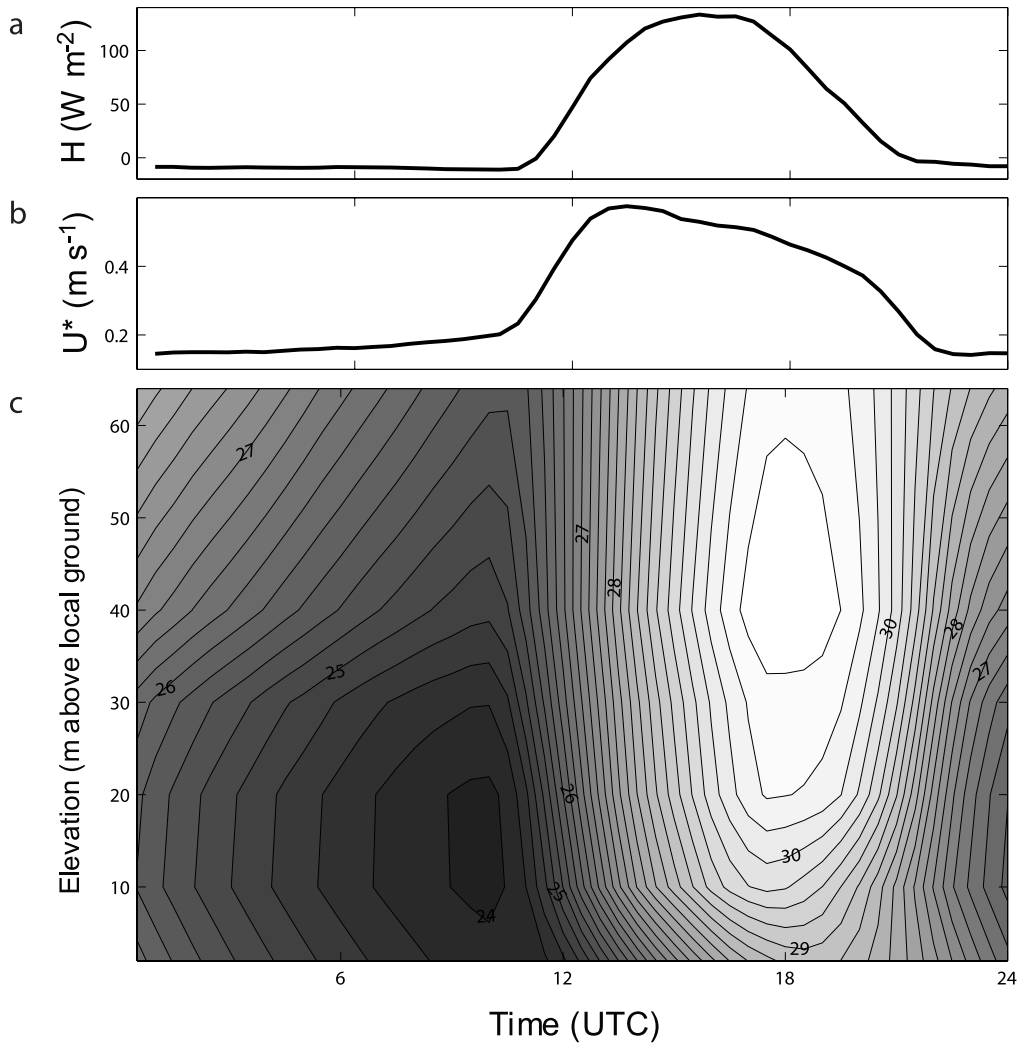

Figure 4. (a) Sensible heat flux at 64 m above ground level (H; W m^{-2}), (b) friction velocity at 64 m above ground level(u*; m s^{-1}), and (c) potential air temperature (°C) from 0 to 64 m above ground level, averaged from 29 June 2000 to 16 January 2004 as a function of UTC. The potential air temperature at sea level was calculated from the observed air temperature assuming a lapse of 0.0098°C m^{-1} and a local ground elevation of 153 m above sea level.

and north, with occasional higher-order stream valleys that were 10 to 90 m deep. The SRTM provides a measure of canopy surface elevation, as indicated by the steps in SRTM elevation at the edges of pastures and roads (Figures 1 and 2). The average SRTM height difference across these borders was 27 m, which we took as the mean SRTM-derived canopy height and used to calculate a ground level elevation at the km-83 tower of 153 m above sea level (asl).

[19] The area within a few km of the tower was flat. The 90-m pixel SRTM elevation within a 1 km radius of the tower ranged from 170 to 191 m asl, with a mean of 180 m and a standard deviation of 4 m (Figure 3). The area around the tower sloped very gently to the west and south. The plateau dropped off into small drainages 1.2 to 1.6 km to the south of the tower and 2.4 to 2.6 km to the west of the tower. The elevation increased slightly to the east and north of the tower. Air draining downhill through the tower site would be expected to flow from the east or north and toward the south, southwest or west.

3.2. Vertical Gradients of Temperature and CO_2 Through the Canopy

[20] The diel patterns of radiation absorption and loss by leaves create repeatable patterns of sensible heat flux, friction velocity, and subcanopy temperature (Figure 4) [see also *Fitzjarrald et al.*, 1990; *Fitzjarrald and Moore*, 1990]. The canopy at km 83 was uneven, with a few large emergents (~55 m) and many gaps and areas with low canopy. The Leaf Area Index (LAI) at the site was high (the annual litterfall at the site was ~5.5 $m^2 m^{-2}$, which implies a comparable LAI if the leaf lifespan is 1 year), and only a small fraction of incident sunlight reached the forest floor. Most of the leaf area was distributed in the lowest 30 m [*Parker and Fitzjarrald*, 2004].

[21] The absorption of sunlight in the upper canopy (20 to 30 m above ground level; agl) created a local source of warm air, generating instability from approximately 20 m agl upward during daytime (Figure 4c), and increasing the above-canopy fluxes of sensible heat and momentum

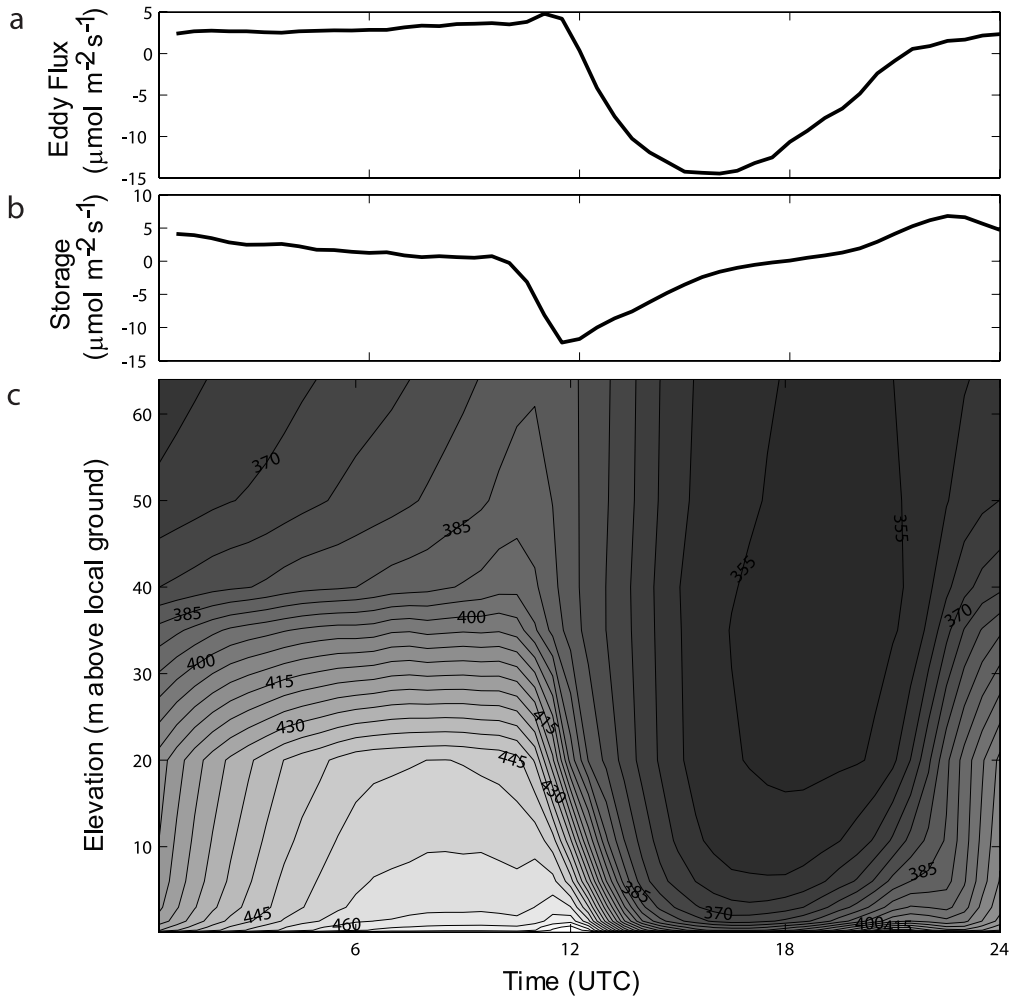

Figure 5. (a) Eddy covariance CO_2 flux at 64 m above ground level (eddy flux; μmol m^{-2} s^{-1}), (b) the change in CO_2 stored in the air column from 0 to 64 m (storage; μmol m^{-2} s^{-1}), and (c) the vertical profile of CO_2 mixing ratio (μmol mol^{-1}) from 0 to 64 m, averaged from 29 June 2000 to 16 January 2004 as a function of UTC.

(Figures 4a and 4b). The canopy atmosphere from ~10 m agl downward was locally stable during daytime. The net loss of thermal radiation at night cooled the canopy relative to the overlying air, which created local stability from 20 to 30 m upward (Figure 4c) and suppressed above-canopy momentum transport (Figure 4b). The vertical profile was divisible into two parcels: an upper warm parcel and a lower cool parcel. The subcanopy parcel was stable with respect to the upper parcel during both the day and night. The top of the lower parcel moved above 20-m agl during the night to include the regions of the canopy where radiation loss was greatest and below 20-m agl during the day to exclude the regions of the canopy where radiation gain was large (Figure 4c).

[22] The concentration of CO_2 in the vertical profile was a function of atmospheric transport and plant metabolism. Photosynthesis during daytime removed CO_2 from the air and resulted in a minimum concentration from ~20 m agl upward (Figure 5). The concentration was particularly high in the lowest ~5 m, presumably as a result of soil and plant sources and because of reduced turbulent transport. The reduction of above-canopy turbulence and the cutoff of photosynthesis at night resulted in a large buildup of CO_2.

[23] The CO_2 concentration in the lowest 20 m was vertically uniform at night (Figure 5c), indicating the subcanopy parcel was well mixed. This subcanopy mixing is consistent with the neutral or slightly unstable temperature gradient observed below the canopy at night (Figure 4c). The combination of radiational cooling from 20 to 30 m upward and warming by heat stored in the soil [*da Rocha et al.*, 2004] apparently generated modest instability beneath the canopy and lead to subcanopy CO_2 mixing. In principle, this process might create a downhill subcanopy flow that could transport CO_2 from the site on clear nights. The lower air parcel might be created when air that has come into contact with radiatively cooled leaves is shed. The creation of cool subcanopy air might then lead to a net downward flow of air from the above-canopy air parcel to the below canopy parcel, which would be balanced by the horizontal flow of subcanopy air to lower topographic areas. This mechanism is similar to that proposed by *Lee* [1998] and is consistent with Figures 4 and 5. A similar mechanism

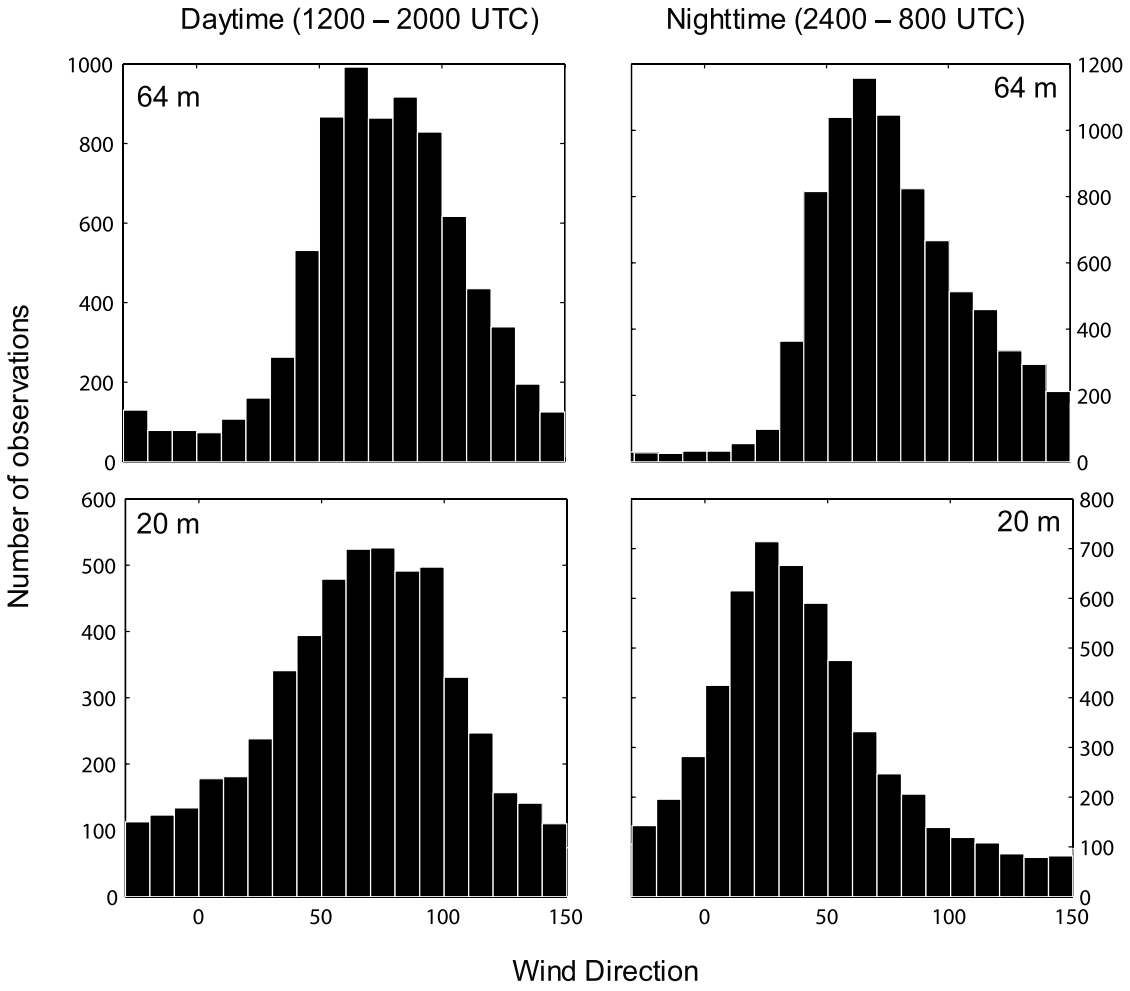

Figure 6. Distribution histograms of wind direction at (top) 64 m agl and (bottom) 20 m agl during (left) daytime (1200–2000 UTC) and (right) nighttime (2400–0800 UTC). Wind direction is in the meteorological convention; 0° indicates wind directly from the north, and 90° indicates wind directly from the east. The bins are 10° wide, and the histograms were determined from the 30-min mean winds that were calculated by averaging the u and v wind components recorded at 1-s intervals from 5 May 2002 to 7 December 2003.

would presumably operate in upslope areas, generating a subcanopy flow that would pass through the site and further contribute to subcanopy CO_2 advection.

3.3. Horizontal Wind in the Canopy

[24] The mean horizontal wind speed during daytime was 2.3 m s^{-1} at 64 m agl, 0.73 m s^{-1} at 30-m agl, 0.23 m s^{-1} at 20-m agl, and 0.09 m s^{-1} at 1.3-m agl (plots not shown). The velocity at 64-m agl remained constant from day to night, while the nocturnal velocity at 30-m agl declined to 0.44 m s^{-1}, the velocity at 20-m agl declined to 0.09 m s^{-1}, and the velocity at 1.3-m agl declined to 0.05 m s^{-1}.

[25] The modal wind direction at 64-m agl was from the east (65°; Figure 6) during both day and night, a pattern that is consistent with the general circulation. A similar pattern was observed at 30-m agl, where the modal wind direction was 75° during daytime and 65° at night (plot not shown). The daytime wind direction at 20-m agl was also from the east, a pattern that is consistent with a tight coupling of air at 20-m agl with that above the canopy (Figures 4 and 5). The wind direction at 20 m agl shifted at night to originate from the northeast (Figure 6), a pattern that is consistent with a decoupling of air beneath the canopy from that above the canopy (Figures 4 and 5). The modal wind direction at 1.3 m shifted from 65 to 75° during daytime to 25 to 35° at night (plot not shown), a pattern that was similar to that observed at 20 m. The nocturnal wind direction shift beneath the canopy to flow from the northeast to the southwest is consistent with the local topography (Figure 3) and a subcanopy flow from upper areas to the north and east of the tower toward lower areas to the south and west of the tower.

3.4. Horizontal Patterns of Land Surface Temperature on Clear Nights

[26] The nocturnal patterns of surface thermal emission (Figure 7) were closely related to local topography and land use (Figures 1 and 2). Similar patterns were observed on all seven nights with cloud-free ASTER images, though the absolute magnitudes and ranges of temperature differed. In

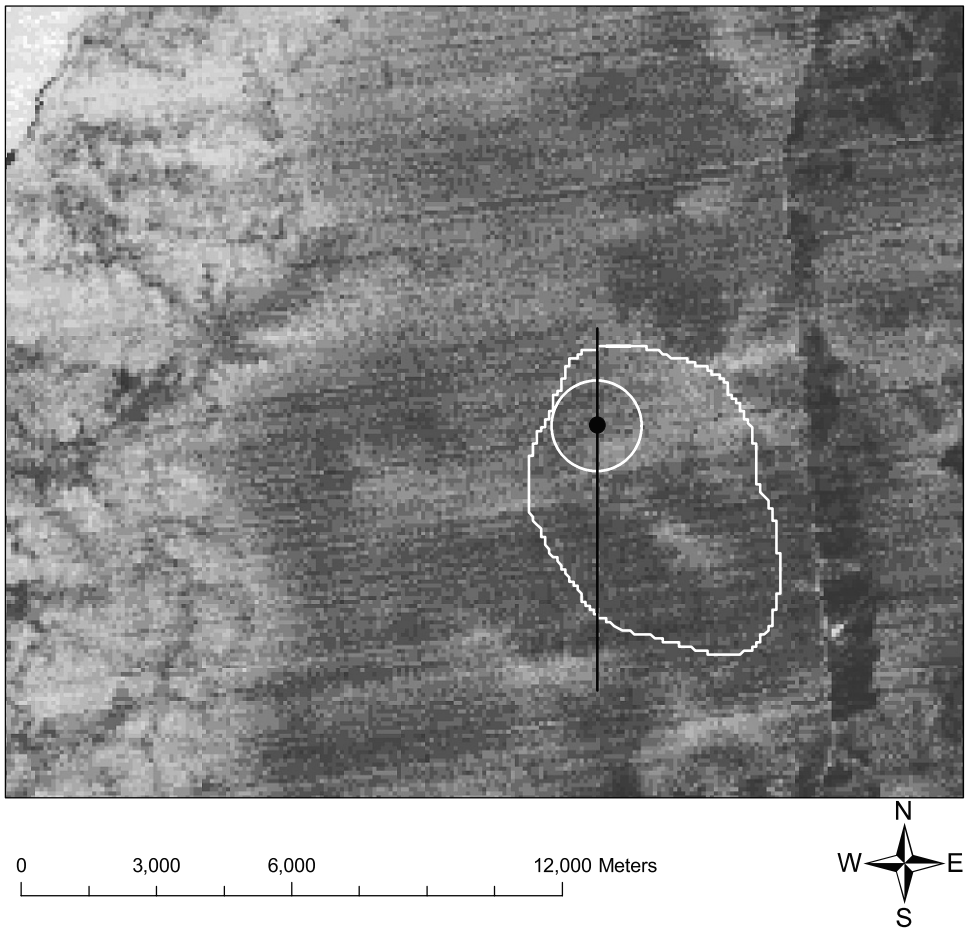

Figure 7. Thermal radiance (ASTER band 10; W m^{-2} μm^{-1} sr^{-1}) measured 21 October 2001, 0218 UTC (20 October 2001, 2218 local time). Areas with higher radiance (warmer surfaces) are lighter; areas with lower radiance are darker.

general, the Tapajos River was warm; the ridges on the escarpment were warm; the drainages on the escarpment were cold; the upper slopes of the escarpment and the edges of the plateau were warm; the center of the plateau was cold; the higher-order stream valleys that dissected the plateau were cold, and the pastures were particularly cold (Figure 7).

[27] The quantitative relationship between ASTER-derived Land Surface Temperature (LST) and elevation was investigated along an 8-km north-to-south transect (Figures 2 and 7). The transect's northern 3.5 km crossed the plateau and the southern 4.5 km traversed a series of higher-order drainages including a creek at 5.7 km (Figure 8). The absolute LST broadly followed the contour, with cooler surface temperatures at lower elevation. The density of vegetation did not vary markedly along the transect. The Normalized Difference Vegetation Index (NDVI) was consistent along the transect (Figure 8), indicating that the change in LST was not an artifact of changes in canopy density and a possible shift in the contribution of soil versus foliage to the LST signal. Rather, the transect observations indicate a nocturnal inversion across the landscape, with cool air pooling in the lower topographic areas. A broadly similar pattern was observed on all seven night with cloud-free ASTER images, though the strength of the inversion differed between nights.

[28] The relationship between elevation and LST along the transect deviated at around 3 km and also at 7.8 km, where anomalous warmth was observed when compared to more central areas of the plateau at comparable elevations (Figure 8). Similar warm belts occurred throughout the ASTER images on the upper slopes of the escarpment and drainages, and extending ~1 to 2 km inward from the edges of the plateau (Figure 7). Thermal belts are well characterized in the literature, and have been recognized for hundreds of years as areas of reduced frost and preferred microclimate for cold intolerant plants (Figure 8) [cf. *Geiger*, 1965]. Thermal belts result when cool air near an edge is drawn downhill by drainage and replaced by the downward movement of warm air from above.

3.5. Relationship Between Horizontal Patterns of LST and in Situ Observations

[29] The relationship between elevation and LST was further analyzed by focusing on a ~30 km^2 area around the tower with 3576 pixels that spanned a range of elevations (Figures 2 and 7). All of the ASTER images indicated decreasing LST with decreasing elevation (Figure 9). The relationship was often curved, with uniformly cool air at a range of elevations below ~150 m (see also Figure 8). The absolute magnitudes of the ASTER-based LSTs were sim-

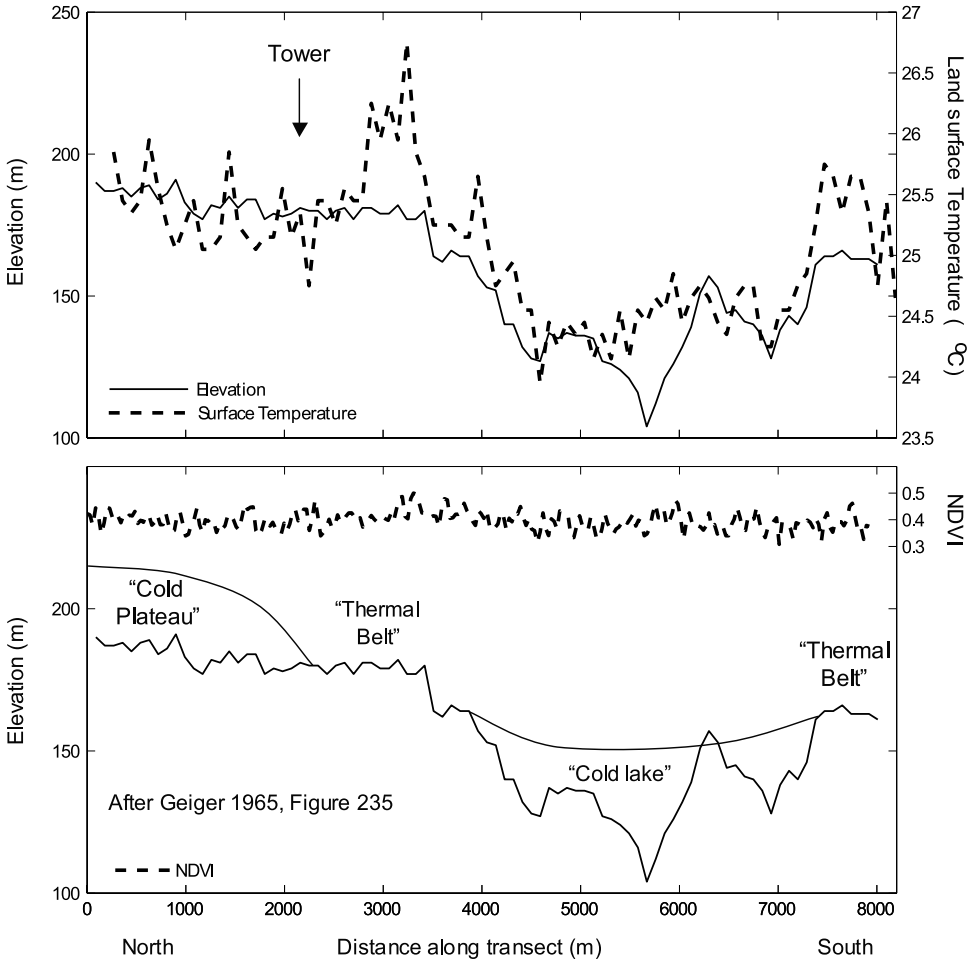

Figure 8. (top) Surface elevation as determined by the SRTM (solid line; m above sea level; lines connect observations at 90-m intervals) and Land Surface Kinetic Temperature (LST; dashed line; °C absolute local temperate; lines connect observations at 90-m intervals) as calculated from ASTER radiance observation on 21 October 2001, 0218 UTC, along the 8 km transect shown in Figure 1. (bottom) Elevation along transect annotated following *Geiger* [1965, Figure 235] (solid line) and the Normalized Difference Vegetation Index (NDVI; dashed line connecting observations at 28.5-m intervals) calculated from the Landsat ETM+ for 30 July 2001 shown in Figure 1.

ilar to the air temperatures observed at the tower (Figure 9; ASTER image from 21 October 2001, 0218 UTC; tower data averaged from 21 October 2001, 0030 to 0230 UTC). The subcanopy air parcel at the tower (the lowest 4 points) was cooler than the LSTs recorded for those elevations in the ASTER image, suggesting a possible flow of subcanopy air to lower-lying areas.

[30] The slope of the relationship between LST and elevation varied between nights, indicating that the degree of thermal stratification, and possibly the extent of cold air drainage, also varied. We took this slope ($\Delta T_{landscape}$) as a measure of the extent of cold air drainage on each night, and tried to relate it to the meteorological conditions at the tower. We hypothesized that $\Delta T_{landscape}$ would differ between nights as a function of friction velocity (u*), with reduced drainage and stratification on nights with a high u*. However, we found no clear relationship between u* and $\Delta T_{landscape}$: calm nights were associated with a range of degrees of stratification (Figure 10a). The lack of a strong relationship between u* and $\Delta T_{landscape}$ remained for a range of meteorological averaging intervals. The relationship was weak if we used the u* calculated for the 30 min period bracketing the satellite overpass, or if we averaged u* for the 2 hours before the overpass (plots not shown).

[31] In contrast, $\Delta T_{landscape}$ was well correlated with the vertical temperature gradient between 64 and 10 m agl measured at the tower (ΔT_{64-10}; Figure 10b). This relationship is not surprising, since Figure 9 implies that the vertical temperature gradient at the tower broadly parallels that observed across the landscape by ASTER. Nonetheless, the relationship between $\Delta T_{landscape}$ and ΔT_{64-10} provides circumstantial evidence that the local stratification at the tower is mechanistically related to the landscape stratification observed by ASTER.

3.6. Relationship Between Tower Flux and Atmospheric Conditions

[32] On the basis of the associations between the in situ observations and LST (Figure 10), we further analyzed the relationship between the net ecosystem exchange (NEE)

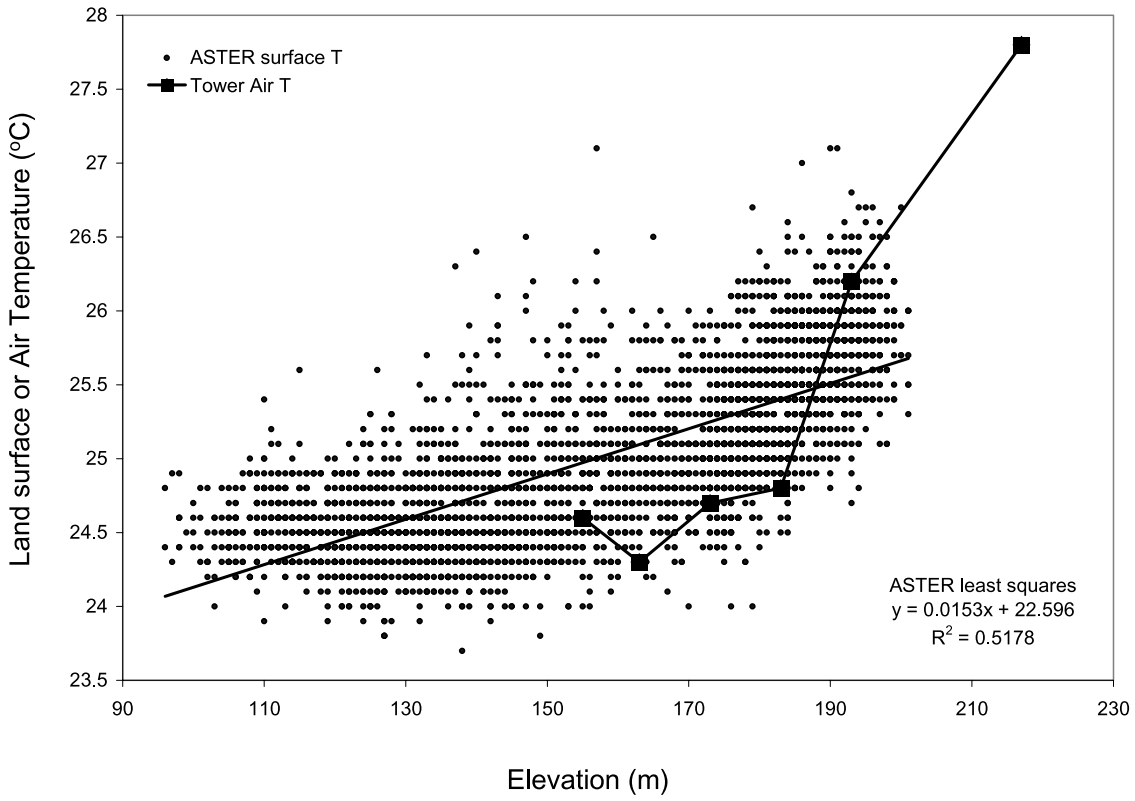

Figure 9. Land Surface Kinetic Temperature (small circles) (LST; °C absolute local temperate; lines connect observations at 90-m intervals) as calculated from ASTER radiance observation on 21 October 2001, 0218 UTC, as a function of surface elevation determined by the SRTM (m above sea level) in the ~30 km^2 region of interest shown in Figure 1. The slope of the relationship between LST and elevation across the landscape (referred to as $\Delta T_{landscape}$ in the text) was 0.0153°C m^{-1}. Air temperature (solid squares) (absolute temperate; not corrected for lapse) averaged from 21 October 2001, 0030 to 0230 UTC, as a function of elevation above sea level.

and meteorological conditions at the tower. We accomplished this analysis by (1) rank ordering the individual nocturnal observations of u* and corresponding NEE by decreasing u*, (2) breaking the data into 10-percentile u* bins with the lowest percentile bin referring to the observations that were best mixed according to the u* criteria, (3) calculating the mean u* and NEE for each bin, and (4) repeating the process for the temperature gradient from 64 and 40 m agl (ΔT_{64-40}). This analysis allowed us to directly compare the relationship between NEE and temperature gradient with that between NEE and u*.

[33] NEE declined markedly with decreasing u* (Figure 11), a pattern that has been observed in many previous investigations. Likewise, NEE declined markedly as ΔT_{64-40} increased, implying a systematic underestimation of CO_2 flux during poorly mixed, stratified conditions. Further analyses (not shown) confirmed that u* and ΔT_{64-40} were well correlated, implying that either measure can be used to screen for the systematic underestimation of flux on calm nights. We therefore suspect that Figure 10 is misleading in the sense that it implies that $\Delta T_{landscape}$ and u* are completely uncorrelated. The tower observations demonstrate that u*, ΔT_{64-40} and ΔT_{64-10} are well correlated, implying that $\Delta T_{landscape}$ and u* are correlated at some level. We suspect that the correlation between $\Delta T_{landscape}$ and u* is weaker than the correlation between $\Delta T_{landscape}$ and $\Delta T_{64-10,}$ and that the $\Delta T_{landscape}$ versus u* relationship in Figure 10 was obscured by the small sample size.

[34] The ideal criteria for screening nocturnal data would show a binary response between the criteria and NEE, with uniformly high NEE when the screening threshold is exceeded and uniformly low NEE for periods below the threshold. This type of binary response would allow for the unambiguous screening of data to exclude bad periods, while minimizing the number of data points that were erroneously identified as good or as bad. While neither u* nor ΔT_{64-40} showed an ideal stepped response, the temperature gradient came closer (Figure 11). NEE was largely independent of ΔT_{64-40} below the 30th percentile, whereas NEE continued to increase with u* in this range. Similarly, the temperature gradient did a better job of identifying the periods with low NEE (e.g., the NEE for poorly mixed periods was consistently lower using ΔT_{64-40} than u*). The landscape analysis (Figure 10) and the tower analysis (Figure 11) both imply that criteria associated with vertical gradients in temperature may prove better than u* for screening nocturnal eddy covariance observations [see also *Staebler and Fitzjarrald*, 2004].

3.7. Evidence of Cold Air Drainage

[35] The total relief within 1 km of the tower was ±10 m (Figure 3), and the site was one of the flattest eddy

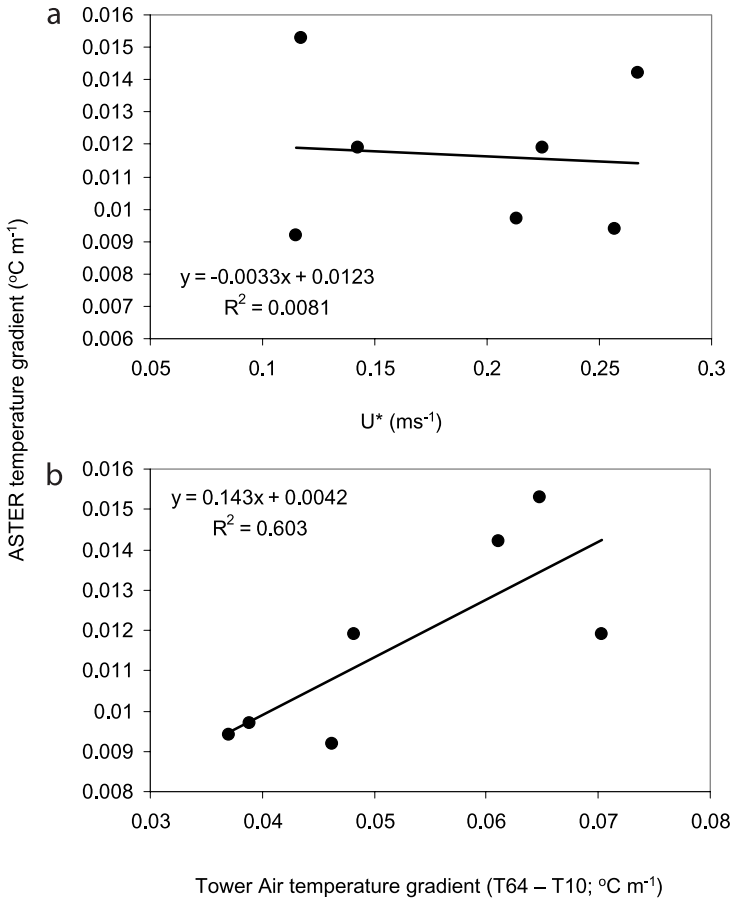

Figure 10. (a) Slope of the relationship between LST and elevation across the landscape ($\Delta T_{landscape}$; °C m^{-1}; calculated as in Figure 7) for the seven nights with clear ASTER images plotted as a function of the friction velocity (u*; m s^{-1}) measured at 64-m above ground level at the km-83 tower averaged for the 2 hours before the satellite overpass. (b) Slope of the relationship between LST and elevation across the landscape ($\Delta T_{landscape}$; °C m^{-1}; calculated as in Figure 7) for the seven nights with clear ASTER images plotted as a function of the temperature gradient from 64-m above ground level to 10 m agl at the km-83 tower (referred to as ΔT_{64-10} in the text) averaged for the 2 hours before the satellite overpass.

covariance installations we have seen. Nonetheless, the site was not flat enough to eliminate problems with the measurement of flux on calm nights: *Miller et al.* [2004] and *Saleska et al.* [2003] reported that the application of a u* filter changed the calculated annual CO_2 exchange at the site from an apparent uptake of ~3.9 Mg C ha^{-1} yr^{-1} to an annual source of ~0.4 Mg C ha^{-1} yr^{-1}.

[36] We believe cold-air drainage removes CO_2 from the site and accounts for the underestimation of CO_2 production on calm, clear nights. The vertical temperature profiles at the km-83 tower (Figures 4 and 9) indicate the subcanopy air is always stable with respect to the upper parcel, raising the possibility that subcanopy air flows downhill at night. The observations of horizontal wind direction (Figure 6) indicate the movement of subcanopy air from the northeast to the southwest. The nocturnal wind direction at 20 m agl differs from that at 40 and 64 m. The nocturnal flow of air at 20 m agl is consistent with the direction that would be expected for cold air flowing to lower topographic regions (Figure 3). The relationship between SRTM elevation and nocturnal ASTER LST and, in particular, the occurrence of thermal belts that extend 1 to 2 km inward from the edges of the plateau (Figures 2 and 7–9) further support the hypothesis that cold air drainage is significant on clear nights. The occurrence of thermal belts around the edges of the plateaus (Figures 7 and 8) implies a net downward motion of air into the canopy space in these areas. Taken in concert, we believe the observations point to the nocturnal flow of air in the lowest 20 m agl toward lower topographic areas to the southwest of the tower.

3.8. Implications for Tropical Forest Carbon Budgets Calculated From Tower Observations

[37] The use of eddy covariance to calculate the carbon budgets of tropical forests has been controversial since *Grace et al.* [1995] and *Malhi et al.* [1998] reported evidence of large carbon uptake by old growth tropical forests. Much of the debate has centered on the possibility of flux underestimation at night, and whether or not flux data should be corrected for a hypothesized loss of CO_2 on calm nights [*Grace et al.*, 1996; *Goulden et al.*, 1996; *Saleska et al.*, 2003; *Miller et al.*, 2004]. Some researchers

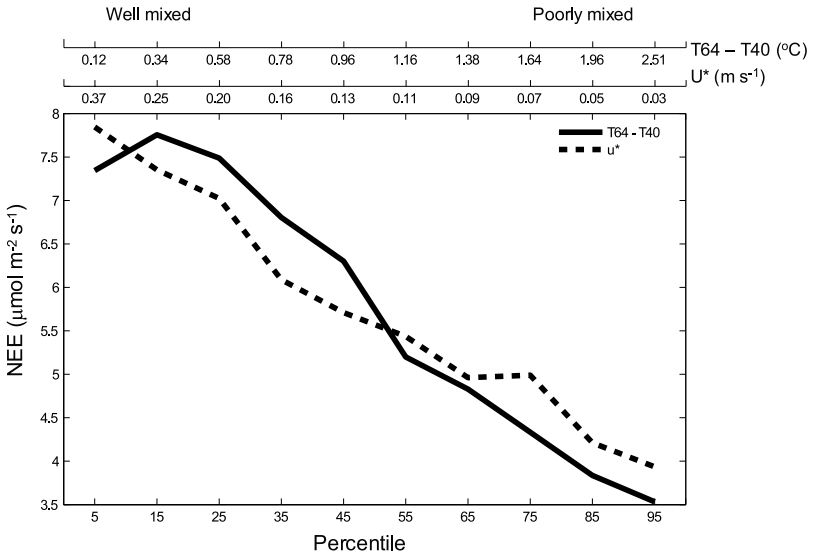

Figure 11. Net ecosystem exchange (NEE) as a function of the friction velocity (u*; m s^{-1}) measured at 64 m (dashed line connecting means within 10 percentile bins). NEE as a function of the temperature gradient from 64 to 40 m agl (ΔT_{64-40}; °C; solid line connecting means within 10 percentile bins). The friction velocities and corresponding NEEs were rank ordered by decreasing u* and broken into 10 percentile bins. The mean NEE for each bin was then calculated and plotted as a function of the u* percentile. The mean u* within each percentile bin was calculated and is shown on a secondary axis. A similar approach was used for the analysis of the temperature gradients. The lowest percentiles for both u* and ΔT_{64-40} indicates the best mixed, least stratified conditions (high u* or low ΔT_{64-40}).

have pointed out that further work is required to fully demonstrate that the CO_2 flux is underestimated on calm nights, and to provide a plausible physical mechanism to account for this underestimation [*Kruijt et al.*, 2004; *Andreae et al.*, 2002; *Araújo et al.*, 2002]. We believe our observations contribute to the growing body of evidence that eddy covariance underestimates the CO_2 flux from tropical forest on calm nights, and that some previous reports of large carbon uptake by old growth tropical forest may be an artifact of the failure to account for the loss of CO_2 by air drainage on calm nights.

[38] **Acknowledgments.** This work was supported by the U.S. National Aeronautics and Space Administration (Goddard NCC5-280; NCC5-702). We thank Dan Hodkinson, Lisa Zweede and Bethany Reed for logistical support; IBAMA, NASA and INPE for agency support; Dave Fitzjarrald for comments on an earlier version of this manuscript; and many others who provided advice and support.

References

Acevedo, O. C., O. L. L. Moraes, R. da Silva, D. R. Fitzjarrald, R. K. Sakai, R. M. Staebler, and M. J. Czikowsky (2004), Inferring nocturnal surface fluxes from vertical profiles of scalars in an Amazon pasture, *Global Change Biol.*, *10*(5), 886–894.

Andreae, M. O., et al. (2002), Biogeochemical cycling of carbon, water, energy, trace gases, and aerosols in Amazonia: The LBA-EUSTACH experiments, *J. Geophys. Res.*, *107*(D20), 8066, doi:10.1029/2001JD000524.

Araújo, A. C., et al. (2002), Comparative measurements of carbon dioxide fluxes from two nearby towers in a central Amazonian rainforest: The Manaus LBA site, *J. Geophys. Res.*, *107*(D20), 8090, doi:10.1029/2001JD000676.

Aubinet, M., B. Heinesch, and M. Yernaux (2003), Horizontal and vertical CO_2 advection in a sloping forest, *Boundary Layer Meteorol.*, *108*(3), 397–417.

Baldocchi, D. D., B. B. Hicks, and T. P. Meyers (1988), Measuring biosphere-atmosphere exchanges of biologically related gases with micrometeorological methods, *Ecology*, *69*(5), 1331–1340.

Baldocchi, D., J. Finnigan, K. Wilson, T. Paw U, and E. Falge (2000), On measuring net ecosystem carbon exchange over tall vegetation on complex terrain, *Boundary Layer Meteorol.*, *96*(1–2), 257–291.

Baldocchi, D., et al. (2001), FLUXNET: A new tool to study the temporal and spatial variability of ecosystem-scale carbon dioxide, water vapor, and energy flux densities, *Bull. Am. Meteorol. Soc.*, *82*(11), 2415–2434.

Black, T. A., et al. (1996), Annual cycles of water vapour and carbon dioxide fluxes in and above a boreal aspen forest, *Global Change Biol.*, *2*(3), 219–229.

da Rocha, H. R., M. L. Goulden, S. D. Miller, M. C. Menton, L. D. V. O. Pinto, H. C. de Freitas, and A. M. E. S. Figueira (2004), Seasonality of water and heat fluxes over a tropical forest in eastern Amazonia, *Ecol. Appl.*, *14*(4), suppl. S, S22–S32.

Feigenwinter, C., C. Bernhofer, and R. Vogt (2004), The influence of advection on the short term CO_2-budget in and above a forest canopy, *Boundary Layer Meteorol.*, *113*(2), 201–224.

Finnigan, J. (1999), A comment on the paper by Lee [1998]: "On micrometeorological observations of surface-air exchange over tall vegetation," *Agric. For. Meteorol.*, *97*(1), 55–64.

Fitzjarrald, D. R., and K. E. Moore (1990), Mechanisms of nocturnal exchange between the rain-forest and the atmosphere, *J. Geophys. Res.*, *95*(D10), 16,839–16,850.

Fitzjarrald, D. R., K. E. Moore, O. M. R. Cabral, J. Scolar, A. O. Manzi, and L. D. D. Sa (1990), Daytime turbulent exchange between the Amazon Forest and the atmosphere, *J. Geophys. Res.*, *95*(D10), 16,825–16,838.

Geiger, R. (1965), *The Climate Near The Ground*, Harvard Univ. Press, Cambridge, Mass.

Goulden, M. L., J. W. Munger, S. M. Fan, B. C. Daube, and S. C. Wofsy (1996), Measurements of carbon sequestration by long-term eddy covariance: Methods and a critical evaluation of accuracy, *Global Change Biol.*, *2*(3), 169–182.

Goulden, M. L., S. D. Miller, H. R. da Rocha, M. C. Menton, H. C. de Freitas, A. M. E. S. Figueira, and C. A. D. de Sousa (2004), Diel and seasonal patterns of tropical forest CO_2 exchange, *Ecol. Appl.*, *14*(4), suppl. S, S42–S54.

Grace, J., et al. (1995), Carbon dioxide uptake by an undisturbed tropical rain forest in southwest Amazonia, *Science*, *270*, 778–780.

Grace, J., Y. Malhi, J. Lloyd, J. McIntyre, A. C. Miranda, P. Meir, and H. S. Miranda (1996), The use of eddy covariance to infer the net carbon dioxide uptake of Brazilian rain forest, *Global Change Biol.*, *2*, 208–217.

Hernandez Filho, P., Y. E. Shimabukuro, and D. C. L. Lee (1993), Final report on the forest inventory project at the Tapajos National Forest, Inst. Nac. De Pesquisas Espaciais, São José dos Campos, Brazil.

Keller, M., et al. (2004), Ecological research in the large-scale biosphere-atmosphere experiment in Amazonia: Early results, *Ecol. Appl.*, *14*(4), suppl. S, S3–S16.

Kruijt, B. J., A. Elbers, C. von Randow, A. C. Arau'jo, P. J. Oliveira, A. Culf, A. O. Manzi, A. D. Nobre, P. Kabat, and E. J. Moors (2004), The robustness of eddy correlation fluxes for Amazon rain forest conditions, *Ecol. Appl.*, *14*, suppl. S, S101–S113.

Lee, X. H. (1998), On micrometeorological observations of surface-air exchange over tall vegetation, *Agric. For. Meteorol.*, *91*(1–2), 39–49.

Malhi, Y., A. D. Nobre, J. Grace, B. Kruijt, M. G. P. Pereira, A. Culf, and S. Scott (1998), Carbon dioxide transfer over a central Amazonian rain forest, *J. Geophys. Res.*, *103*, 31,593–31,612.

Massman, W. J., and X. Lee (2002), Eddy covariance flux corrections and uncertainties in long-term studies of carbon and energy exchanges, *Agric. For. Meteorol.*, *113*(1–4), 121–144.

McMillen, R. T. (1988), An eddy-correlation technique with extended applicability to non-simple terrain, *Boundary Layer Meteorol.*, *43*(3), 231–245.

Miller, S. D., M. L. Goulden, M. C. Menton, H. R. da Rocha, H. C. de Freitas, A. M. E. S. Figueira, and C. A. D. de Sousa (2004), Biometric and micrometeorological measurements of tropical forest carbon balance, *Ecol. Appl.*, *14*(4), suppl. S, S114–S126.

Parker, G., and D. R. Fitzjarrald (2004), Canopy structure and radiation environment metrics indicate forest developmental stage, disturbance, and certain ecosystem functions, paper presented at III LBA Scientific Conference, Braz. Minist. of Sci. and Technol., Brasilia, Brazil, July.

Radke, L. F., and A. C. Delany (2002), The role of quantitative infrared imagery in investigations of the nocturnal boundary layer, *J. Atmos. Oceanic Technol.*, *19*(11), 1783–1792.

Saleska, S. R., et al. (2003), Carbon in Amazon forests: Unexpected seasonal fluxes and disturbance-induced losses, *Science*, *302*(5650), 1554–1557.

Staebler, R. M., and D. R. Fitzjarrald (2004), Observing subcanopy CO_2 advection, *Agric. For. Meteorol.*, *122*(3–4), 139–156.

Tans, P. P., I. Y. Fung, and T. Takahashi (1990), Observational constraints on the global atmospheric CO_2 budget, *Science*, *247*(4949), 1431–1438.

Turnipseed, A. A., D. E. Anderson, P. D. Blanken, W. M. Baugh, and R. K. Monson (2003), Airflows and turbulent flux measurements in mountainous terrain, part 1. Canopy and local effects, *Agric. For. Meteorol.*, *119*(1–2), 1–21.

Valentini, R., et al. (2000), Respiration as the main determinant of carbon balance in European forests, *Nature*, *404*(6780), 861–865.

Wan, Z. (1999), MODIS Land-Surface Temperature Algorithm Theoretical Basis Document (LST ATBD), version 3.3, NASA, Greenbelt, Md. (Available at http://modis.gsfc.nasa.gov/data/atbd/land_atbd.php)

Wofsy, S. C., M. L. Goulden, J. W. Munger, S. M. Fan, P. S. Bakwin, B. C. Daube, S. L. Bassow, and F. A. Bazzaz (1993), Net exchange of CO_2 in a midlatitude forest, *Science*, *260*(5112), 1314–1317.

H. R. da Rocha, Department of Atmospheric Sciences, University of Sao Paulo, Sao Paulo, SP 05508-900, Brazil.

M. L. Goulden and S. D. Miller, Department of Earth System Science, University of California, Irvine, CA 92697-3100, USA. (mgoulden@uci.edu)